Anisotropic superconductivity and frozen electronic states at the (111) $LaAlO_3/SrTiO_3$ interface

S. Davis,[1] Z. Huang,[2,3] K. Han,[2,3] Ariando,[2,3,4] T. Venkatesan,[4,2,5,6,7] and V. Chandrasekhar[1,*]

[1]*Graduate Program in Applied Physics and Department of Physics and Astronomy, Northwestern University, 2145 Sheridan Road, Evanston, Illinois 60208, USA*

[2]*NUSNNI-Nanocore, National University of Singapore 117411, Singapore*

[3]*Department of Physics, National University of Singapore 117551, Singapore*

[4]*NUS Graduate School for Integrative Sciences & Engineering, National University of Singapore 117456, Singapore*

[5]*Department of Physics, National University of Singapore 117542, Singapore*

[6]*Department of Electrical and Computer Engineering, National University of Singapore 117576, Singapore*

[7]*Department of Material Science and Engineering, National University of Singapore 117575, Singapore*

(Received 3 August 2017; revised manuscript received 28 May 2018; published 9 July 2018)

We report measurements of the superconducting properties of the two-dimensional (2D) gas that forms at the interface between $LaAlO_3$ (LAO) and $SrTiO_3$ (STO) in the (111) crystal orientation, a system that permits *in situ* tuning of carrier density and disorder by means of a back-gate voltage V_g. Like the (001) oriented LAO/STO interface, superconductivity at the (111) LAO/STO interface can be tuned by V_g. The 2D superconductivity in these (111) LAO/STO samples shows an in-plane anisotropy, being different along different interface crystal directions, and "remembers" the disorder landscape at which they are cooled through the superconducting transition. The low energy scale and other characteristics of this memory effect distinguish it from charge-trapping effects previously observed in (001) interface samples.

DOI: 10.1103/PhysRevB.98.024504

I. INTRODUCTION

Superconductors with exotic order parameter symmetries quite often exhibit rich phase diagrams filled with nontrivial magnetic states [1], charge states [2], and even nematic order [3–5]. On the other hand, conventional, *s*-wave metallic superconductors show no such complexity, and are expected to be isotropic [6], although some *s*-wave superconductors such as MgB_2 are thought to have anisotropic gaps [7]. More recently, superconductivity has been extensively investigated in the conducting interface that forms between the two band insulators LAO and STO in the (001) crystal orientation [8–11]. The unique feature of this two-dimensional (2D) system is that the properties of the interface can be modified by simply changing the voltage V_g on a gate [9–11], enabling tuning of the superconductivity with an *in situ* experimental handle. While this tunability with V_g has been used extensively to investigate the nature of the 2D superconductivity at the interface, all indications to date are that the superconducting order is of an isotropic, conventional *s*-wave type [9–11]. Additionally, tunneling measurements have provided some evidence that the superconductivity at the interface is unconventional in character [12,13].

The crystal symmetry of the (001) oriented LAO/STO interface at room temperature is C_4. The crystal symmetry of the (111) oriented LAO/STO interface at room temperature is C_3 [14,15]. This hexagonal symmetry has led to predictions of novel properties in the normal and superconducting properties of the 2D conducting gas (2DCG) at the (111) LAO/STO interface [14–16]. In particular, Boudjada *et al.* [14] have predicted emergent magnetic and in-plane nematic order in the normal state resulting from broken rotational symmetry at the interface, driven in part by multiorbital and spin-orbit interactions. The electronic nematicity in the normal state manifests itself as an anisotropy with respect to crystal surface direction that is observed in almost all the electronic properties of the (111) interface, including the longitudinal resistance, Hall effect, and quantum capacitance [17–20]. At lower temperatures, the nematicity is predicted to manifest itself as an anisotropy in the superconducting properties of the (111) LAO/STO interface [15]. We show below that the superconducting properties of the (111) LAO/STO interface are indeed anisotropic, being different when measured along different surface crystal directions. In view of the prediction by Scheurer *et al.* [16] that superconductivity at the (111) LAO/STO interface, in contrast to (001) and (110) LAO/STO interfaces, breaks time reversal symmetry, this may point to the existence of an unconventional superconducting order parameter.

In addition, we find that the normal and superconducting properties as well as the anisotropy at temperatures $T \lessapprox T_c$ strongly depend on the gate voltage at which the sample is cooled from ≈ 4 K, even if the gate voltage is subsequently changed at lower temperatures. The freezing effect is an indication of disorder that can be frozen in at very low temperatures in these structures by the application of a gate voltage, and which can be reversed by warming the sample to temperatures above a freezing temperature $T_F \approx 1$ K. The behavior is distinctly different in energy scale and qualitative response to V_g from the charge trapping behavior reported earlier in (001) LAO/STO interface samples [9,21–23]. While other groups

*v-chandrasekhar@northwestern.edu

 ©2018 American Physical Society

have reported observing superconductivity in (111) oriented LAO/STO interfaces, the two effects we report here point to the potentially exotic nature of the superconducting correlations in this system [24,25].

II. SAMPLE FABRICATION AND MEASUREMENT

The heterostructures used in this work consisted of 20 monolayers (ML) of LAO grown epitaxially on Ti terminated (111) STO substrates by pulsed laser deposition. Details of the film synthesis can be found in our previous work [17,18]. On each 5 mm × 5 mm chip, 4 Hall bars (600 μm × 100 μm) were fabricated using a combination of photolithography and Ar ion milling such that two of the Hall bars were oriented along the $[1\bar{1}0]$ surface crystal direction, and the remaining two were oriented along the $[\bar{1}\bar{1}2]$ surface crystal direction, as shown in the inset to Fig. 1(a). Chips were then exposed to different post-growth annealing processes to change their global carrier densities. Half of the devices were annealed in an O_2 atmosphere and the other half in an Ar/H_2 atmosphere in processes identical to those described in Ref. [16]. Annealing in an O_2 environment reduces the number of oxygen vacancies and hence reduces the carrier concentration, while annealing in Ar/H_2 increases the oxygen vacancy concentration and hence increases the carrier concentration; however, both types of samples have overall 2D carrier densities on the order of $10^{13}/cm^2$ [18].

A total of 10 Hall bars on three different chips were measured at milli-Kelvin temperatures using both an Oxford Kelvinox MX100 and Kelvinox 300 dilution refrigerator; here we report data on the four Hall bars for which we have the most comprehensive data. To measure the transport characteristics of the samples we utilized custom home-built amplifiers and high impedance current sources in conjunction with traditional lock-in techniques, allowing for measurement of sample impedances of up to a GΩ. To maintain a uniform protocol for all data discussed here, the gate voltage was applied at a temperature of 4.4 K before cooling down to 30 mK, unless otherwise noted. V_g was then repeatedly cycled between ±100 V to obtain reproducible curves before the data reported here were taken. The data discussed here are primarily for two freezing voltages $V_F = -10$ V and $V_F = 50$ V for which we took the most extensive data. Data for other voltages (e.g., $V_F = 0$ V) follow the expected trend.

In order to measure T_c continuously as a function of V_g we have employed a feedback technique which utilizes an ac resistance bridge and home-built proportional-integral-differential (PID) temperature controller to maintain a specific sample resistance via temperature control. We chose the sample resistance (750 Ω) to be at the foot of the superconducting transition, and balance the ac resistance bridge at this point. The output of the bridge is then input to the PID which controls a heater at the mixing chamber of the dilution refrigerator. As V_g is swept, the PID changes the heater power and therefore the sample temperature in order to minimize the error signal from the bridge. V_g must be swept slowly enough for the sample temperature to equilibrate with the mixing chamber temperature. An indication that this equilibrium was reached is the lack of hysteresis in the sweeps shown in Fig. 5(b); consequently, each sweep took in excess of 20 h.

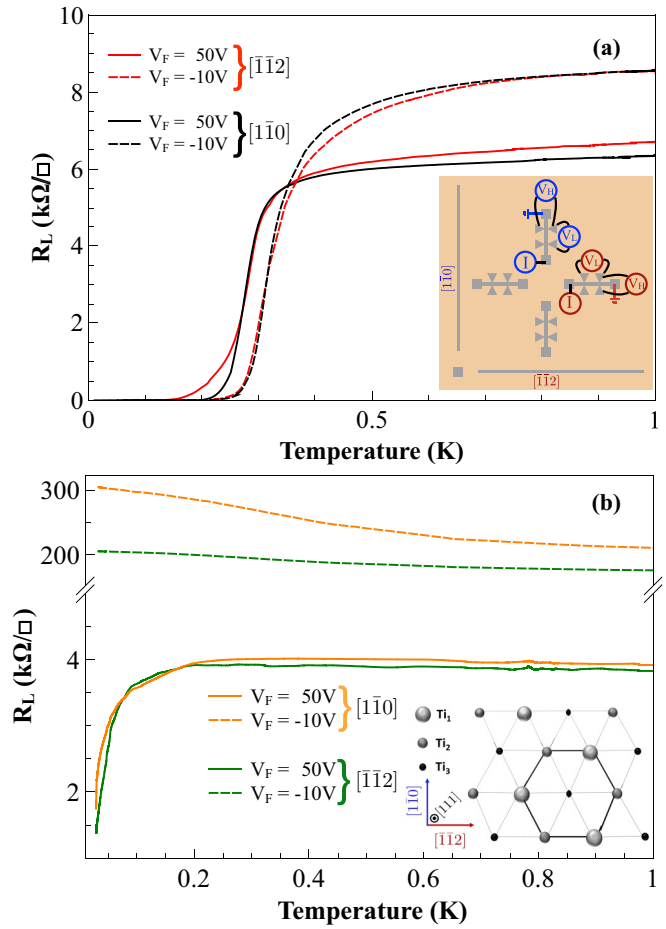

FIG. 1. Resistance as a function of temperature with different freezing voltages V_F along two crystal directions. (a) The Ar/H_2 annealed samples show full superconducting transitions. While the normal state resistance R_N is higher for $V_F = -10$ V, the superconducting transition temperature T_c is also higher. (b) The O_2 annealed samples do not go superconducting, but show hints of a superconducting transition for $V_F = 50$ V, and insulating behavior for $V_F = -10$ V, with strong anisotropy between the the $[\bar{1}\bar{1}2]$ and $[1\bar{1}0]$ crystal directions in the latter. Inset in (a) is a schematic of the Hall bars on each sample chip, which shows the measurement configuration. Inset in (b) is a schematic representation of the crystal structure at the interface for the first three layers of Ti atoms. The atoms are designated by the size of the atoms as well as the labels $Ti_{1,2,3}$ and represent the Ti atoms ranging from the interface to 2 layers below the interface.

III. EXPERIMENTAL RESULTS

In (111) LAO/STO interface structures, the normal state transport characteristics (longitudinal resistance, Hall coefficient, and quantum capacitance) are strongly anisotropic [17–20], being different along the $[\bar{1}\bar{1}2]$ and $[1\bar{1}0]$ directions, the anisotropy increasing with decreasing oxygen vacancy concentration and more negative V_g [18]. While in-plane anisotropy in transport characteristics has also been observed in (001) LAO/STO interface structures, and has been variously ascribed to microstructural effects [26] or ferroelectric twin domains walls [27–29], the in-plane anisotropy in the

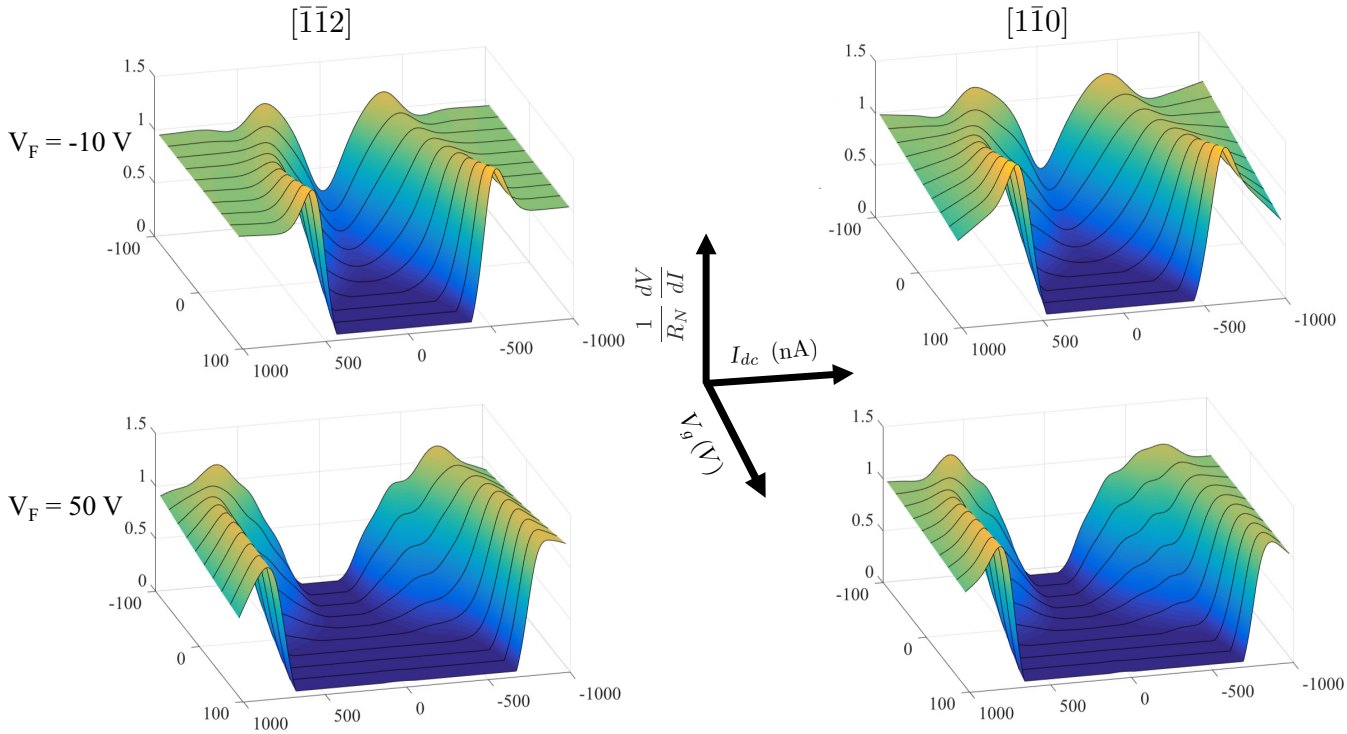

FIG. 2. Differential resistance of the Ar/H_2 annealed samples at 30 mK, for $V_F = -10$ V and $V_F = 50$ V, and both surface crystal orientations. The critical current I_c varies with V_g, a consequence of electrostatic doping by the gate, but is also a function of the freezing voltage V_F applied while cooling through the superconducting transition: in general, I_c is larger for $V_F = 50$ V in comparison to $V_F = -10$ V. For the Ar/H_2 annealed devices, there is relatively little anisotropy between the two crystal directions. Due to the large variation in R_N with V_g, the curves here and in Fig. 3 are normalized to the value of dV/dI at ± 1 μA.

(111) devices is characteristically different in magnitude and qualitative behavior, and thus has a different origin. This has been discussed in detail in Refs. [15,16], but we discuss these differences here for emphasis. First, the maximum in-plane anisotropy observed in the (001) structures is at most a factor of 2, while the anisotropy observed in the (111) structures an order of magnitude at the most negative gate voltages measured, and continues to increase with decreasing V_g. Second, the anisotropic behavior is consistent across a number of different samples grown with different parameters and across multiple cool downs from room temperature: for example, the longitudinal resistance along the $[1\bar{1}0]$ direction is always higher than the resistance along the $[\bar{1}\bar{1}2]$ direction at large negative gate voltages, so that effects such as the specific orientation of step edges on the surface of a sample cannot explain the anisotropy we observe [this is one explanation for the small anisotropy seen in (001) LAO/STO samples] [26]. This is also an argument against the effect of ferroelectric twin domains walls [27], which would be randomly oriented from run to run. Third, no anisotropy is observed at liquid nitrogen temperatures (77 K), indicating that the structural transition that occurs at $\approx$105 K [30] in STO, which is another explanation that has been put forward for the (001) samples, also cannot explain our results. (Indeed, the anisotropy onsets at $T \sim 22$ K, far from any structural transition in the STO [20].) Finally, the hexagonal symmetry at the (111) interface might at first sight lead one to expect a difference between the $[1\bar{1}0]$ and $[\bar{1}\bar{1}2]$ crystal directions; however, further thought shows that this is not the case, as the underlying lattice still has cubic symmetry. Thus, the large in-plane anisotropy observed in (111) LAO/STO devices in the longitudinal resistance, Hall effect, and quantum capacitance is characteristically different from any anisotropic effects seen previously in (001) devices. As we noted above, Boudjaja *et al.* [14] predict that orbital and spin interactions at the (111) interface may lead to charge and/or spin ordering and an emergent nematic phase, but this topic is just beginning to be explored theoretically. We discuss below low temperature data in the superconducting regime for two sets of samples, one set annealed in an Ar/H_2 atmosphere after fabrication, and the other in an O_2 atmosphere. As discussed above and in previous publications, the post-growth treatment affects the oxygen vacancy concentration and hence the resistivity of the 2DCG, and, as we demonstrate here, the superconducting properties as well.

Figures 1(a) and 1(b) show the superconducting transitions of an Ar/H_2 annealed sample and an O_2 annealed sample with two different back-gate "freezing" voltages $V_F = -10$ V and $V_F = 50$ V applied as the samples were cooled through the transition. The Ar/H_2 annealed samples showed a superconducting transition, with V_F affecting both the normal state resistance R_N and the superconducting transition T_c. The O_2 annealed samples did not go fully superconducting: there is a hint of a superconducting transition for $V_F = 50$ V, while insulating behavior is seen for $V_F = -10$ V, with clear anisotropy in resistance between the two crystal directions (a much stronger anisotropy is observed at lower gate voltages)

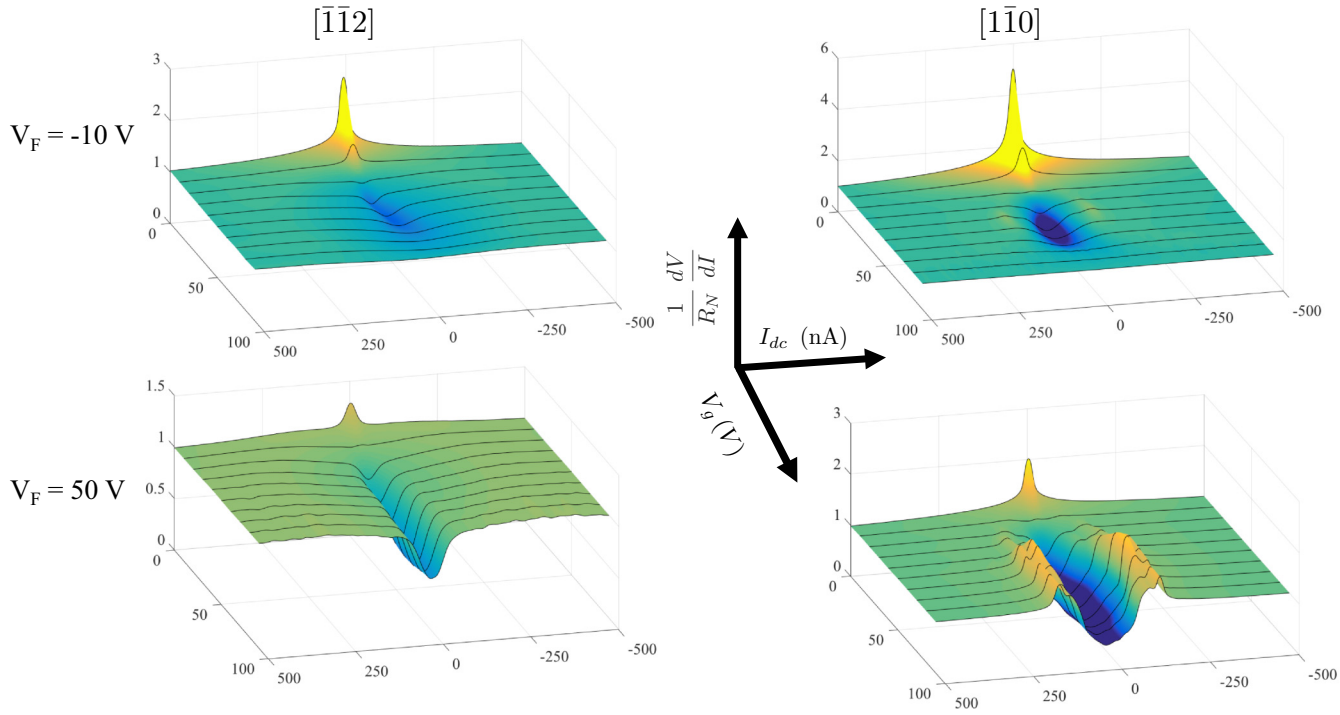

FIG. 3. Differential resistance of the O_2 annealed samples at 30 mK, for $V_F = -10$ V and $V_F = 50$ V, for both surface crystal directions. While the O_2 annealed samples do not go fully superconducting, there is clear evidence for incipient superconductivity in the current-voltage characteristics, even for $V_F = -10$ V, for which the resistance increases with decreasing temperature [Fig. 1(b)]. As with the Ar/H_2 annealed samples (Fig. 2), the superconducting characteristics change with V_g, a consequence of electrostatic doping, but also are a function of the voltage V_F at which they are cooled. For the O_2 annealed samples, the superconducting characteristics are also highly anisotropic, being very different along the two crystal directions, as has been reported earlier for other transport properties [17,18]. Clear evidence for a maximum in superconducting properties as a function of V_g (the superconducting "dome") can also be seen.

[17,18]. However, it should be noted that when there is a full or partial superconducting transition as a function of temperature in either the Ar/H_2 or O_2 annealed samples, the transition temperatures measured along the two different crystal directions are similar, although the transition along the $[\bar{1}\bar{1}2]$ direction in the Ar/H_2 annealed samples is in general broader. Thus, it appears at first sight that the superconducting properties are fairly isotropic, even though the normal state properties are quite anisotropic. We will show later that some of the properties of the superconducting state are quite anisotropic, but we would first like to focus on the dependence of the superconducting properties on the applied gate voltage.

It is not surprising that the superconducting transition temperature depends on gate voltage. A similar dependence of the superconducting properties on gate voltage has been reported in (001) LAO/STO structures [11], and is ascribed to electrostatic doping of the electron gas. Unlike the (001) structures, part of the difference in the (111) LAO/STO devices is due to trapped states frozen in by the application of a gate voltage at higher temperatures.

The difference between electrostatic doping and frozen disorder can be seen clearly in the normalized nonlinear differential resistance dV/dI as a function of dc current I_{dc} and gate voltage V_g at temperatures far below T_c, shown in Fig. 2 for the Ar/H_2 annealed samples. As expected, the critical current I_c varies with V_g, being in general smaller for more negative V_g. This is the effect of electrostatic doping with V_g, similar to that observed previously in the (001) LAO/STO samples [11]. Additionally, as we have explored in our earlier work the nonlinear differential resistance in the Ar/H_2 annealed samples is weakly anisotropic, especially near I_c [24]. However, the most striking feature of these data is that the current-voltage characteristics also depend on the gate voltage V_F at which the samples were cooled, even when V_g is subsequently repeatedly changed over the same range. The difference is persistent: as noted in Sec. II, data were taken after the gate voltage had been swept repeatedly between ± 100 V at 30 mK; the sample remembers the voltage V_F at which it was cooled. Figure 3 shows similar data for the O_2 annealed samples. Here the samples do not go completely superconducting, although a dip in the differential resistance can clearly be seen over a certain range of V_g, mimicking the dome observed in (001) LAO/STO samples [9,11]. Even so, the freezing effect is quite clear: in both crystal directions, the drop in differential resistance near zero bias along both crystal directions is much larger for $V_F = 50$ V than for $V_F = -10$ V. Just as striking as the freezing effect is the obvious anisotropy present between the two in-plane crystal directions that is seen most clearly when comparing the two crystal directions with $V_F = 50$ V. When cooled in this configuration the dip in nonlinear differential resistance is much broader in the $[1\bar{1}0]$ direction than in the $[\bar{1}\bar{1}2]$.

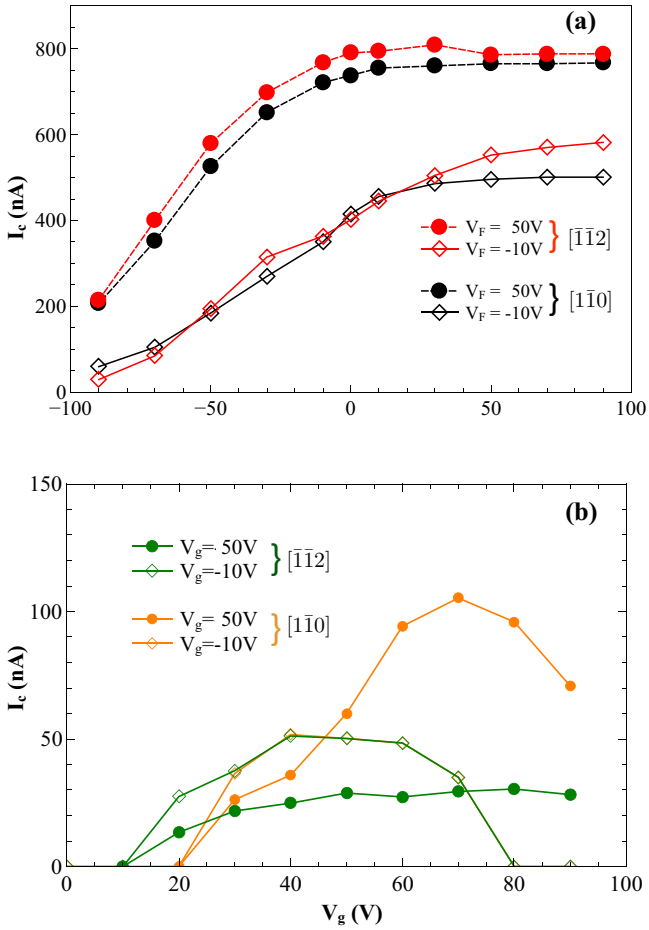

FIG. 4. Critical current I_c for the Ar/H_2 annealed samples (a) and the O_2 annealed samples (b) for freezing voltages $V_F = -10$ V and $V_F = 50$ V, for both surface crystal directions, taken from Figs. 2 and 3, respectively. Since the data show multiple peaks, I_c is defined to be the value of I_{dc} at which the slope of dV/dI vs I_{dc} is a maximum ($d^3V/dI^3 = 0$).

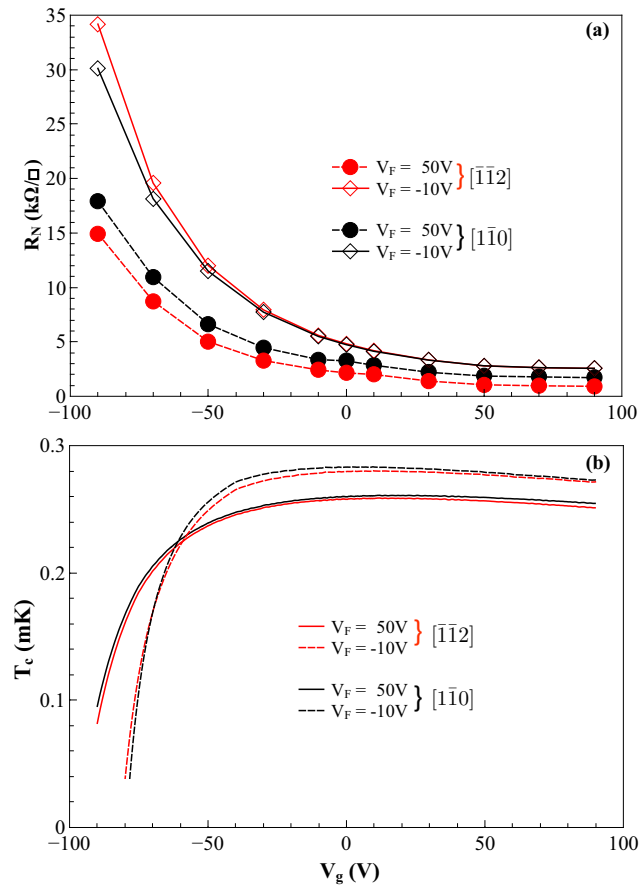

FIG. 5. Normal state resistance (a) for the Ar/H_2 annealed samples for freezing voltages $V_F = -10$ V and $V_F = 50$ V, for both the and crystal directions, taken from Fig. 2. Since the data show multiple peaks R_N is defined as the value of dV/dI at $I_{dc} \pm 1$ μA. (b) Critical temperature T_c as a function of V_g for the Ar/H_2 annealed samples, measured as described in Sec. II.

A different representation of the data of Figs. 2 and 3 is given in Figs. 4(a) and 4(b), which show the critical current I_c as a function of V_g for the Ar/H_2 and O_2 annealed samples, respectively. For the Ar/H_2 annealed samples, I_c shows a broad maximum, in effect, a saturation, at positive V_g, occurring at around $V_g \approx 0$ V for $V_F = 50$ V, and $V_g = 100$ V for $V_F = -10$ V. However, I_c's for $V_F = -10$ V are approximately a factor of 2 smaller than those for $V_F = 50$ V. Thus, setting a gate voltage $V_F = -10$ V as the sample is cooled through its transition results in lower critical currents over the entire gate voltage range in comparison to $V_F = 50$ V. More interestingly, the dependencies of the two freezing voltages cannot be scaled to each other simply by shifting the traces along the V_g axis, again showing that we are tuning more than the carrier density of the interface. Further examination of the data for the Ar/H_2 annealed samples in Fig. 2 is given in Fig. 5(a), which shows the normal state resistance R_N as a function of V_g for the Ar/H_2 annealed samples. In general, R_N increases rapidly with decreasing V_g, as expected, but the sharp upturn in R_N occurs at larger V_g for $V_F = -10$ V in comparison to $V_F = 50$ V. However, T_c shows a different trend [Fig. 5(b)]. T_c is lower for $V_F = -10$ V than for $V_F = 50$ V for $V_g - 60$ V, but uniformly larger above this value. This trend of an increase of T_c coupled with a decrease in I_c has also been observed in Al films [31,32], and has been associated there with a modification with disorder of the attractive electron-phonon interaction responsible for superconductivity [33,34]. On the other hand, when the O_2 annealed samples are cooled with $V_F = -10$ V, the superconducting properties show a domelike behavior in I_c for $0 \leqslant V_g \leqslant 80$ V; I_c vanishes outside this range. When the O_2 annealed samples are cooled with $V_F = 50$ V, the behavior of I_c is drastically different along the two crystal directions, clearly showing the anisotropy between the two directions. This drastic change, not only in amplitude but also in V_g dependence, suggests that we may be tuning the shape of the superconducting phase diagram and not just the carrier density.

From these data, it is evident that applying a back-gate voltage V_F as the sample is cooled through its transition freezes in a specific configuration that influences the normal and superconducting state properties at very low temperatures, even if V_g is subsequently swept. The configuration is stable in time over a scale of a week, and robust against changes in I_{dc}

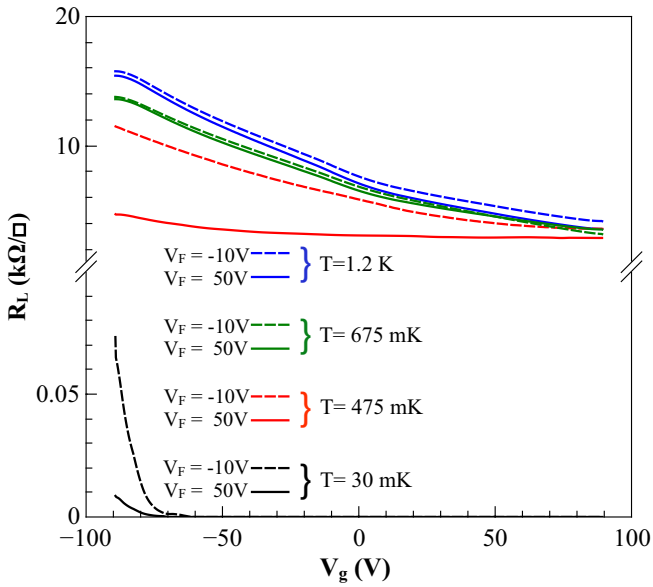

FIG. 6. Onset of the freezing transition. Resistance of the Ar/H_2 annealed samples in the $[\bar{1}\bar{1}2]$ crystal orientation as a function of V_g after cooling from 4.4 K to the target temperatures noted with gate voltages $V_F = -10$ V and $V_F = 50$ V applied. As the resistance is hysteretic with V_g, the average of the upsweep and downsweep traces as a function of V_g is shown in each case. Differences between the curves for the two freezing temperatures show up only below 600–700 mK, showing that the freezing temperature T_F is of order ∼0.6 K.

and magnetic field in addition to V_g, so long as the temperature is not raised above a certain freezing temperature T_F. In order to determine T_F, we cooled the devices down from 4.4 K to a target temperature with gate voltages of either $V_F = -10$ V or $V_F = 50$ V applied, and then measured the resistance as a function of V_g. After each resistance measurement, the sample was warmed to 4.4 K before another measurement was made. Traces of R_L vs V_g for four target temperatures of 30 mK, 470 mK, 675 mK, and 1.2 K are shown in Fig. 6. Furthermore, due to the hysteretic nature of R_L vs V_g traces we have shown the average of the upsweep and downsweep traces as a function of V_g. We have previously shown that averaging the up and downsweeps accurately represents the long time scale behavior of the system [17].

For simplicity, we have shown data for only the Ar/H_2 annealed devices in the $[\bar{1}\bar{1}2]$ crystal direction: At 1.2 K and 675 mK there is only a small difference in the resistance as a function of V_g. At 470 mK, the difference is much larger, almost a factor of 5 at negative V_g. Finally, at 30 mK, the difference is almost an order of magnitude at negative V_g (the sample is superconducting for $V_g \geqslant -40$ V at this temperature). Thus, the temperature at which the configuration is frozen in is $T_F \approx 1$ K.

In (001) LAO/STO interface samples, the resistance at low temperature depends on the history of how V_g is swept after first cooling the sample down from room temperature, eventually settling into a hysteretic but reproducible behavior as a function of V_g. This has been ascribed to an irreversible change in the occupation of charge states near the interface that can only be reset by warming to room temperature, indicating that the relevant energy scales for population or depopulation of these charge states are of that order (≈25 meV) [21]. We also observe a similar initial, irreproducible, history dependence of the properties in the (111) interface samples on first cooling down from room temperature, after which the properties as a function of V_g become hysteretic but reproducible. However, the freezing effects in the (111) interface samples reported here are different, in that different values and V_g dependencies of I_c, R_N, and T_c can be stabilized at very low temperature depending on the freezing voltage V_F without introducing new irreproducible dependencies at these temperatures. Furthermore, these frozen states set/reset at a very low energy scale, ≈1 K. This temperature is far lower than many of the phase transitions observed in the system, structural or otherwise. For instance, a structural transition to a disordered tetragonal phase is what ostensibly drives the irreversible population of charge states discussed above and occurs at ≈105 K. This temperature scale is also much lower than the temperature (∼22 K) below which nematic order nucleates in the normal state [20].

Nevertheless, it may be possible that the freezing effect is associated with other trapped states with much lower energy scales. From Fig. 5, it appears that shifting the $V_F = 50$ V curves towards positive V_g would roughly align the curves for the two different freezing temperatures, although the shifts would be different for R_N. However, it is clear that even with shifting one of the curves, the superconducting properties cannot be made to align, as the saturation values of I_c and T_c at large V_g for the two freezing temperatures are quite different, implying that we are changing the shape of the superconducting phase diagram. Consequently, it is clear that the effects that we observe are not solely due to residual electric fields due to trapped charges, at least with regard to the superconducting properties: the effects we observe, particularly the increase in T_c for $V_F = -10$ V, similar to what is observed in Al films, suggests that increased disorder due to the trapped charges may be important. This disorder is predicted to strongly affect the nematic state at the interface and may drive it from a spin-density wave to a charge-density wave [14]. If the freezing of charged trap states is indeed responsible for the freezing effect we observe at 1 K, one would need to understand the very low energy scales of these states. Uncovering the origin of these low energy scales will require further experimental and theoretical work.

Finally, we return to the question of the anisotropy of the superconducting properties with respect to surface crystal direction. As we noted above, the full or partial superconducting transition as a function of temperature is not strongly anisotropic for either the Ar/H_2 or O_2 annealed samples (Fig. 1). However, the superconducting nonlinear differential resistance measured at low temperatures is anisotropic. This is most evident in the data for the O_2 annealed samples show in Fig. 3, in particular for $V_F = 50$ V, and is reflected in the plot of I_c vs V_g shown in Fig. 5(b). The anisotropy in the Ar/H_2 annealed samples is much weaker but still present, consistent with earlier observations that the anisotropy is weaker in samples of lower resistance [17,18]. As there have been no reports of anisotropy in the superconducting characteristics of (001) LAO/STO structures, as well as doped STO devices, consistent with the expected *s*-wave character of superconductivity in these systems, the anisotropy observed

here is unexpected, and may point to the exotic nature of superconductivity at the (111) interface.

In summary, low temperature measurements of the (111) LAO/STO interface show superconducting behavior with an unexpected in-plane anisotropy, pointing to a potentially exotic form of superconductivity. The very low temperature behavior is also influenced by disorder that is frozen in by cooling the devices in different electric fields; changing not only the superconducting properties on the samples, but the anisotropy as well.

ACKNOWLEDGMENTS

Work at Northwestern was funded through a grant from the U.S. Department of Energy through Grant No. DE-FG02-06ER46346. Work at NUS was supported by the MOE Tier 1 (Grants No. R-144-000-364-112 and No. R-144-000-346-112) and Singapore National Research Foundation (NRF) under the Competitive Research Programs (CRP Awards No. NRF-CRP8-2011-06, No. NRF-CRP10-2012-02, and No. NRF-CRP15-2015-01).

[1] W. J. Gannon, W. P. Halperin, C. Rastovski, K. J. Schlesinger, J. Hlevyack, M. R. Eskildsen, A. B. Vorontsov, J. Gavilano, U. Gasser, and G. Nagy, New J. Phys. **17**, 023041 (2015).

[2] S. Kasahara, H. J. Shi, K. Hashimoto, S. Tonegawa, Y. Mizukami, T. Shibauchi, K. Sugimoto, T. Fukuda, T. Terashima, Andriy H. Nevidomskyy, and Y. Matsuda, Nature (London) **486**, 382 (2012).

[3] R. A. Borzi, S. A. Grigera, J. Farrell, R. S. Perry, S. J. S. Lister, S. L. Lee, D. A. Tennant, Y. Maeno, and A. P. Mackenzie, Science **315**, 214 (2007).

[4] M. G. Kim, R. M. Fernandes, A. Kreyssig, J. W. Kim, A. Thaler, S. L. Bud'ko, P. C. Canfield, R. J. McQueeney, J. Schmalian, and A. I. Goldman, Phys. Rev. B **83**, 134522 (2011).

[5] H. Kotegawa, S. Kawasaki, A. Harada, Y. Kawasaki, K. Okamoto, G.-Q. Zheng, Y. Kitaoka, E. Yamamoto, Y. Haga, Y. Onuki, K. M. Itoh, and E. E. Haller, J. Phys. Condens. Matter **15**, S2043 (2003).

[6] P. W. Anderson, J. Phys. Chem. Solids **11**, 26 (1959).

[7] C. Buzea and T. Yamashita, Supercond. Sci. Technol. **14**, R115 (2001).

[8] N. Reyren, S. Gariglio, A. D. Caviglia, D. Jaccard, T. Schneider, and J.-M. Triscone, Appl. Phys. Lett. **94**, 112506 (2009).

[9] A. D. Caviglia, S. Gariglio, N. Reyren, D. Jaccard, T. Schneider, M. Gabay, S. Thiel, G. Hammerl, J. Mannhart, and J.-M. Triscone, Nature (London) **456**, 624 (2008).

[10] S. Thiel, G. Hammerl, A. Schmehl, C. W. Schneider, and J. Mannhart, Science **313**, 1942 (2006).

[11] D. A. Dikin, M. Mehta, C. W. Bark, C. M. Folkman, C. B. Eom, and V. Chandrasekhar, Phys. Rev. Lett. **107**, 056802 (2011).

[12] C. Richter, H. Boschker, W. Dietsche, E. Fillis-Tsirakis, R. Jany, F. Loder, L. F. Kourkoutis, D. A. Muller, J. R. Kirtley, C. W. Schneider, and J. Mannhart, Nature (London) **502**, 528 (2013).

[13] D. Stornaiuolo, D. Massarotti, R. Di Capua, P. Lucignano, G. P. Pepe, M. Salluzzo, and F. Tafuri, Phys. Rev. B **95**, 140502(R) (2017).

[14] N. Boudjada, G. Wachtel, and A. Paramekanti, Phys. Rev. Lett. **120**, 086802 (2018).

[15] D. Doennig, W. E. Pickett, and R. Pentcheva, Phys. Rev. Lett. **111**, 126804 (2013).

[16] M. S. Scheurer, D. F. Agterberg, and J. Schmalian, NPJ: Quantum Mater. **2**, 9 (2017).

[17] S. Davis, V. Chandrasekhar, Z. Huang, K. Han, Ariando, and T. Venkatesan, Phys. Rev. B **95**, 035127 (2017).

[18] S. K. Davis, Z. Huang, K. Han, Ariando, T. Venkatesan, and V. Chandrasekhar, Adv. Mater. Interfaces **4**, 1600830 (2017).

[19] P. K. Rout, I. Agireen, E. Maniv, M. Goldstein, and Y. Dagan, Phys. Rev. B **95**, 241107(R) (2017).

[20] S. K. Davis, Z. Huang, K. Han, Ariando, T. Venkatesan, and V. Chandrasekhar, Phys. Rev. B **97**, 041408(R) (2018).

[21] Z. Q. Liu, D. P. Leusink, X. Wang, W. M. Lu, K. Gopinadhan, A. Annadi, Y. L. Zhao, X. H. Huang, S. W. Zeng, Z. Huang, A. Srivastava, S. Dhar, T. Venkatesan, and Ariando, Phys. Rev. Lett. **107**, 146802 (2011).

[22] C. Bell, S. Harashima, Y. Kozuka, M. Kim, B. G. Kim, Y. Hikita, and H. Y. Hwang, Phys. Rev. Lett. **103**, 226802 (2009).

[23] J. Biscaras, S. Hurand, C. Feuillet-Palma, A. Rastogi, R. C. Budhani, N. Reyren, E. Lesne, J. Lesueur, and N. Bergeal, Sci. Rep. **4**, 6788 (2014).

[24] S. K. Davis, Z. Huang, K. Han, Ariando, T. Venkatesan, and V. Chandrasekhar, Phys. Rev. B **96**, 134502 (2017).

[25] A. M. R. V. L. Monteiro, D. J. Groenendijk, I. Groen, J. de Bruijckere, R. Gaudenzi, H. S. J. van der Zant, and A. D. Caviglia, Phys. Rev. B **96**, 020504(R) (2017).

[26] P. Brinks, W. Siemons, J. E. Kleibeuker, G. Koster, G. Rijnders, and M. Huijben, Appl. Phys. Lett. **98**, 242904 (2011).

[27] H. J. Harsan Ma, S. Scharinger, S. W. Zeng, D. Kohlberger, M. Lange, A. Stöhr, X. Renshaw Wang, T. Venkatesan, R. Kleiner, J. F. Scott, J. M. D. Coey, D. Koelle, and Ariando, Phys. Rev. Lett. **116**, 257601 (2016).

[28] A. Buckley, J. P. Rivera, and E. K. H. Salje, J. Appl. Phys **86**, 1653 (1999).

[29] M. Honig, J. A. Sulpizi, J. Drori, A. Joshua, E. Zeldov, and S. Ilani, Nat. Mater. **12**, 1112 (2013).

[30] R. Mizaras and A. Loid, Phys. Rev. B **56**, 10726 (1997).

[31] B. Abeles, R. W. Cohen, and G. W. Cullen, Phys. Rev. Lett. **17**, 632 (1966).

[32] M. Nittmann, P. Ziemann, W. Buckel, and G. Linker, Z. Phys. B - Condens. Matter **41**, 205 (1981).

[33] P. G. De Gennes, Rev. Mod. Phys. **36**, 225 (1964).

[34] J. W. Garland, K. H. Bennemann, and F. M. Mueller, Phys. Rev. Lett. **21**, 1315 (1968).